Deep-learning-enabled crack detection and analysis in commercial lithium-ion battery cathodes

Tianyu Fu[1,2,†], Federico Monaco[3,†], Jizhou Li[4,*], Kai Zhang[1,*], Qingxi Yuan[1,*], Peter Cloetens[3], Piero Pianetta[4], Yijin Liu[4,*]

1. Beijing Synchrotron Radiation Facility, X-ray Optics and Technology Laboratory, Institute of High Energy Physics, Chinese Academy of Sciences, Yuquan Road, Shijingshan District, Beijing 100043, China
2. University of Chinese Academy of Sciences, Yuquan Road, Shijingshan District, Beijing 100043, China
3. European Synchrotron Radiation Facility, Grenoble 38000, France
4. Stanford Synchrotron Radiation Lightsource, SLAC National Accelerator Laboratory, Menlo Park, CA 94025, USA

[†]These authors contributed equally to this work: Tianyu Fu, Federico Monaco.

*Correspondence and requests for materials should be addressed to J. Li (lijz@slac.stanford.edu), K. Zhang (zhangk@ihep.ac.cn), Q. Yuan (yuanqx@ihep.ac.cn), and Y. Liu (liuyijin@slac.stanford.edu).

Abstract

In Li-ion batteries, the mechanical degradation initiated by micro cracks is one of the bottlenecks for enhancing the performance. Quantifying the crack formation and evolution in complex composite electrodes can provide important insights into electrochemical behaviors under prolonged and/or aggressive cycling. However, observation and interpretation of the complicated crack patterns in battery electrodes through imaging experiments are often time-consuming, labor intensive, and subjective. Herein, we develop a deep learning-based approach to extract the crack patterns from nanoscale hard X-ray holo-tomography data of a commercial 18650-type battery cathodes. We demonstrate efficient and effective quantification of the damage heterogeneity with automation and statistical significance. We further associate the crack characteristics with the active particles' packing densities and discuss a potentially viable architectural design for suppressing the structural degradation in an industry-relevant battery configuration.

Keywords: Li-ion battery; crack detection; deep learning; X-ray holo-tomography; Phase contrast.

1. Introduction

Li-ion batteries (LIBs) are electrochemical systems, increasingly used for powering portable electronics and electric vehicles. Their high energy density and good cycling performance make them outperform many other energy storage solutions. However, further increase in energy density, power density, life-time, and safety need to be persistently pursued due to the growing demands in various application. Chemomechanical breakdown is an important fading mechanism in LIBs that affects many aspects of battery performance. It has been broadly reported in almost all LIB's components including anode, solid-electrolyte interphase, and cathode [1–4]. An in-depth understanding and quantification of the crack formation and distribution in a statistically meaningful manner can direct the future research for reducing the detrimental effects and improving the manufacturing procedures.

In this work, we utilize micro- and nano-scale X-ray tomography to image the inner structure of an electrochemically abused 18650-type cylindrical cell. The cracking phenomenon in commercial cells is of particular interest to this industry because the manufacturing procedure is often already "optimized" through trial-and-errors. Nevertheless, it has been reported that, in commercial cells, poor mechanical robustness and deactivation of cathode particles and particle clusters due to contact failure could arise in the presence of non-uniform packing [5]. In another work, it was reported that the delaminated region in the cathode could be associated with severe particle cracking [6]. To establish a deeper understanding with statistical significance and, subsequently, to make an informed improvement in electrode manufacturing, crack detection and analysis

with automation is pivotal. To achieve this goal, material scientists need to leverage novel developments in advanced computing.

Machine learning, especially deep learning, has been widely adopted for material research due to its inherent capability in processing massive data and high-dimensional analysis. For instance, Jiang et al. [7] proposed a deep convolutional neural network approach to segment thousands of battery particles, which facilitates the statistical analysis, showing that active particles of different size would detach from the conductive matrix differently. This development, however, cannot be directly applied to the crack detection in our case due to the irregularity of the particle's morphology in our sample.

Herein, we develop a deep-learning method for automatically identifying the cracks in the tomographic images of composite cathode retrieved from a commercial cell. Specifically, a state-of-the-art U-Net-based neural network [8] is trained and applied to our data. Each slice of the tomography data is processed separately and then the 3D crack distribution is assembled by merging all the slices. Our method provides an efficient yet precise segmentation for the 3D crack network.

We demonstrate the effectiveness of our approach by mapping the heterogeneous degradation in an electrochemically abused 18065-type battery cathode [9,10]. We associate the local damage density with the corresponding packing density, which reveals a depth-dependent profile. Our approach for large-scale high-throughput crack detection eliminates the potentially biased conclusion yield from conventional labor-intensive manual analysis. We anticipate that the developed technique and the resulting findings

could critically inform the design of electrodes from commercial LIBs with better performance.

2. Materials and Methods

2.1 Nanoscale synchrotron phase-contrast holotomography

Synchrotron X-ray phase contrast imaging (XPCI) generates image contrast stemming from X-ray phase shift induced by the sample, which could provide substantially improved sensitivity. It is particularly powerful for imaging the light (low-Z) materials, e.g., carbon and binder domains in composite battery cathode [11]. Hence both the transition metal oxides (the active cathode particles, $LiNi_xMn_yCo_{1-x-y}O_2$) and the porous carbon and binder matrix can be visualized with adequate quantitative sensitivity [7,9]. To investigate the micromorphology of LIB cathode with high spatial resolution down to the nanoscale, the X-ray phase contrast holotomography measurements were performed at the ID16A-NI nano-imaging beamline at the European Synchrotron Radiation Facility (ESRF) in Grenoble, France. This beamline features a high-energy hard X-ray nano-probe, which delivers a brilliant flux (up to 10^{12} photons s^{-1} at $\Delta E/E \approx 1\%$) within a nano-focus down to ~20 nm. Its unique performance was implemented through two pairs of advanced multilayer-coated Kirkpatrick–Baez (KB) optics, operating at 17 and 33.6 keV respectively. Our LIB cathode sample was placed downstream of the KB focus under the illumination of 33.6 keV X-rays. Magnified holograms were acquired by a FReLoN charged-coupled device camera with 4096 × 4096 pixels of 1.5 μm binned in 2x2 mode. The large magnification of the cone beam geometry leads to an effective pixel size at ~70 nm. One entire phase contrast nano-tomographic volume was obtained acquiring the data at four different sample-to-focus distances. For every distance, 2000 projections were

recorded with 0.2 second exposure time. The projections collected at the four distances were used in the phase retrieval process to reconstruct the corresponding 2D phase map for each angle [12]. The retrieved 2D phase maps were subsequently fed into a tomographic reconstruction algorithm using classical filtered back projection (ESRF PyHST software package [13]). The grey levels in each voxel of the resulting 3D volumes are proportional to the real part of the complex refractive index, which is governed by the local distribution of the electron density in the sample.

2.2 Architecture of the U-Net based deep learning approach

The deep learning network used here exhibits a U-Net based deep convolutional architecture [8]. The effectiveness of U-Net, especially with limited training dataset, has been demonstrated in many applications [14–17]. The crack detection network is a typical full convolution network, which is composed of an encoder and a decoder. The detailed structure of the network is shown in **Fig. S1**. Firstly, the 2D slices extracted from the 3D reconstruction of the electrode are fed into the network. The encoder network compress each raw image into a set of “features” that represent the morphological characteristics of the cracks. The encoder network is composed of five convolution modules, and each convolution module consists of two 3x3 convolution layers and the ReLU activation function [18]. The convolution modules are connected by a maximum pooling layer [19]. The function of the maximum pooling layer is to down-sample the input data in order to reduce the computational cost of the network. Then the encoded data is decoded by the decoder network, which progressively optimizes the crack detection results. The decoder network is also composed of four convolution modules. Each convolution module is connected through up-sampling convolution. In addition, the decoder network is

connected with the encoder through the skip-connection structure, which provides sufficient context information that further improves the accuracy.

The training and verification process of the network is shown in **Fig. 2**. In our implementation, the training dataset has 48 images and the verification set has 16 images. All the images are 512x512 pixels, and they are randomly selected by slicing the 3D volume at different depths and in different orientations. We note here that thanks to the U-net architecture and the data augmentation strategies, i.e., a series of random changes such as rotation, scaling, cropping, etc., the network model is well trained and performs remarkably well on unseen images. We define the loss function of the network as the sigmoid cross-entropy [20], which can evaluate the detection results of the network and quantify the error. The crack detection network is implemented on the TensorFlow framework. The built network was deployed on a workstation with 2.2 GHz Intel Xeon silver 4114 CPU and NVIDIA Quadro p6000 graphics processor (GPU).

3. Results and discussion

3.1 Multi-scale structural hierarchy of an 18650-type battery

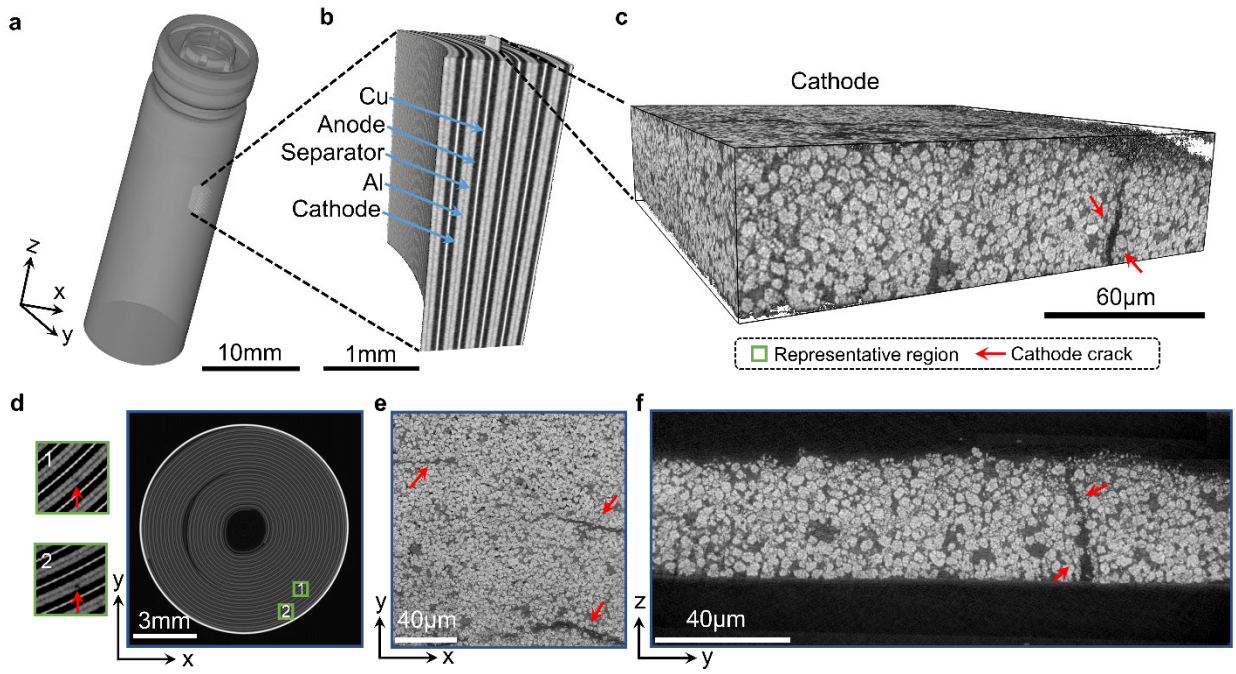

Fig. 1. The multi-scale structural hierarchy of an 18650 Li-ion battery cell. (a-b) The 3D rendering and a zoomed-in region of the microtomographic data of the cell. (c) A randomly selected sub-volume of the cathode obtained from synchrotron nano-resolution phase-contrast holotomography. (d) 2D slice of the reconstructed volume in (a). Two regions of interest showing cathode cracks are enlarged in the left insets. (e) and (f) The 2D vertical and horizontal slices of the reconstructed volume in (c), respectively. The cathode cracks are highlighted by red arrows.

We carried out an X-ray overview of the 18650-type battery cell using microtomography [6]. As shown in **Figs.1a-b**, the jelly roll structure of the cell can be clearly visualized. The cathode, which consists of $LiNi_{0.5}Mn_{0.3}Co_{0.2}O_2$ (NMC532), and the anode's Cu current collector show strong contrast, while the graphite anode and the cathode's Al current collector are relatively transparent. We further disassembled the cylindrical cell in an

argon-filled glovebox and harvested the regions of interest as identified by our microtomographic overview of the cell. The recovered regions of interest are then scanned using synchrotron-based nano-resolution holotomography. In our experiment, a spatial resolution at 70-100 nm with quantitative phase contrast was achieved, allowing us to visualize and quantify the delaminated regions and cracked NMC particles in greater details. As shown in **Figs. 1e-f,** the cathode of this cell is made of irregularly-shaped secondary particles at 3-4 μm. They are fairly closely packed and their damaging degrees are quite heterogeneous.

This particular commercial cell is intended for fast-charging applications. Therefore, active particles with small size were used for reducing the lithium diffusion length and promoting the reaction kinetics during the fast-charging process. The observed intra-secondary-particle cracks originated from the electrochemical cycling are even smaller, at ~1 μm or smaller. Another thing to highlight is that our holotomography data covers a large field-of-view (at ~500x500 μm). This offers very rich information regarding the spatial heterogeneity of the electrochemical behavior, chemomechanical breakdown, and the active particle packing. It is, however, challenging to manually segment the particle cracks or to use conventional image processing algorithms for this task. In this context, the herein developed deep-learning approach becomes essential to effectively and faithfully analyze the imaging data with both large field of view and high resolution.

3.2 Deep-learning-based automatic crack detection

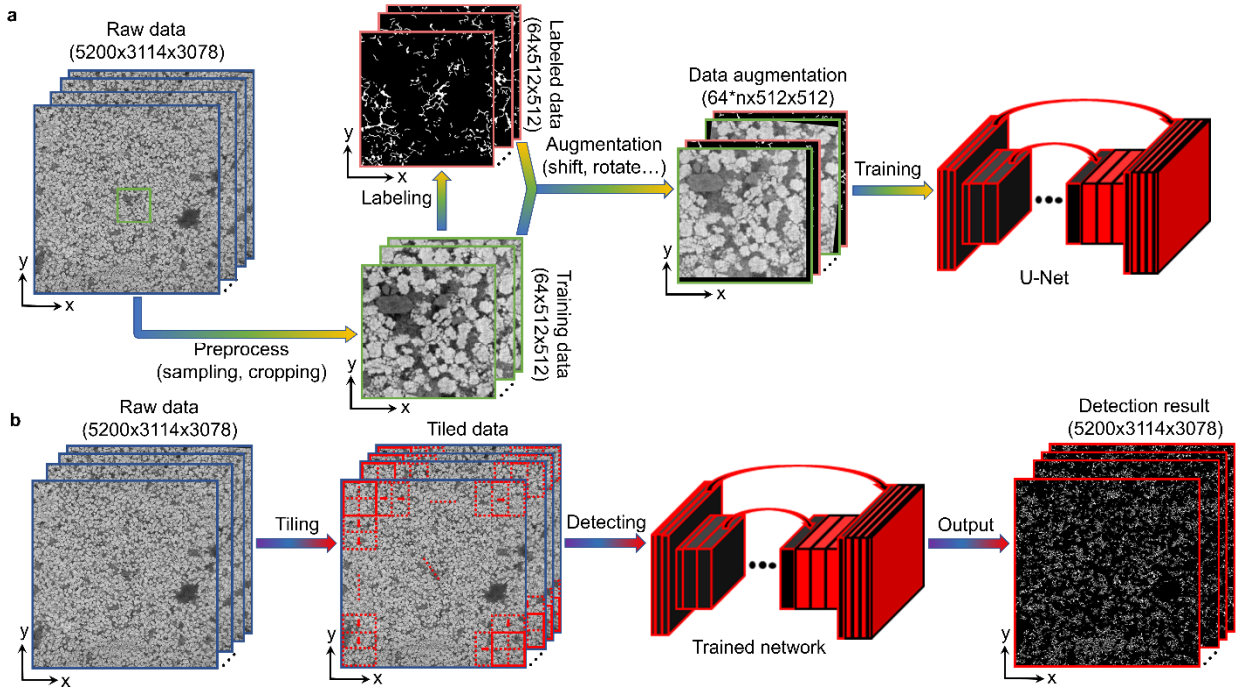

Fig. 2. The pipeline of the proposed deep-learning-based method for detecting the particle cracks in the holotomography data. (a) A small set of 2D images is extracted from the 3D data volume for training the neural network. Training data is manually labeled and further augmented through shift, rotation, cropping, etc. The U-Net architecture is adapted in our framework. (b) The trained model is applied to the large images tile-by-tile and the final result is obtained through fusing the detection results for all the tiles.

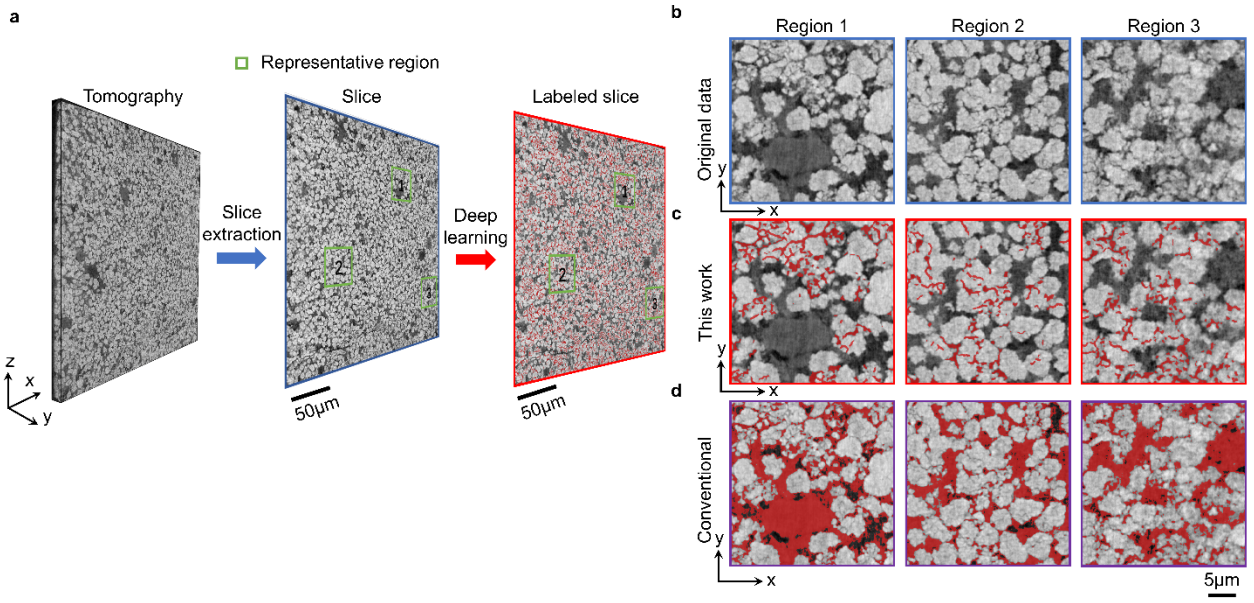

Fig. 3. Representative examples of the crack detection results and the comparison against that of a conventional approach. (a) The trained model is applied to each slice of the tomography data and an overview of the crack distribution is obtained. (b) Three selected regions. (c) and (d) The corresponding crack detection results obtained by our deep-learning method and the conventional image-intensity-based segmentation approach, respectively.

To perform quantitative and statistical analysis of the particle cracks in these images, we build a set of automatic identification models based on the deep neural network technique. The whole pipeline of our framework is shown in **Fig.2**. Specifically, a small set of the raw images is preprocessed by cropping into subsets of 512x512 blocks. We labeled the particle cracks manually to obtain the ground truth for the training and validation purposes. We used 75% of the manually labeled data as the training data and the rest was used as the testing set to evaluate the network performance. To enrich the training set and to

improve the generalizability of the trained model, we performed the data augmentation by translating, rotating and scaling the image blocks. This step acts as a regularizer and helps reduce overfitting and, subsequently, boosts the network performance. Finally, we applied the well-trained model to the original data using a sliding window and stitched the results to obtain the final output. Compared with directly working with the full-size image or the 3D data, the adopted strategy can reduce the required the computing resources dramatically. The training and validation losses are presented in **Fig. S2**.

With this deep-learning-based detection method, we accurately quantify and analyze the crack level for a large number of NMC particles in the imaged volume. As shown in **Fig.3a**, each slice from the tomography data is extracted and the trained model is applied to obtain the crack distribution. Three randomly selected regions are presented in **Fig.3b**, and their corresponding detection results by our method are shown in **Fig.3c**. All particle cracks can be accurately identified and even for those challenging regions (i.e. void and segregation of carbon/binder) are handled properly. To verify the advantage of our method, we compare to the conventional thresholding-based image segmentation algorithms, which is shown in **Fig. 3d**. Conventional approach clearly failed to separate the crack and void regions, whereas our deep learning approach demonstrates significantly improved performance. This shows that the trained model can almost achieve the human-eye performance and replace the large amount of labor required for conventional manual labeling.

3.3 Quantification of heterogeneous degradation in composite battery cathode

Build upon our deep-learning-based method, we quantified the crack level from the particle level to the electrode level. The shapes of these particles are irregular and they

are tightly packed and heterogeneously fragmented. We choose to evaluate a moving window of 50x50 pixels, and use the quantified crack area to color-code the image forming a damage density map.

We first compare the top and bottom layers in the electrode (the lateral virtual slices are shown **Figs.4a** and **4b**; ~5 μm from the top surface, close to separator, and ~5 μm from the bottom surface, near the aluminum current collector, respectively) and two selected regions are enlarged for better visualization. The cracks in both layers are automatically identified using the deep learning method. The respective damage density maps are calculated and shown in **Figs.4c** and **4d**, respectively. Overall, the particles close to the separator show more severe morphological damage than those close to the current collector. To further quantify this phenomenon, we plot the cracking profile across different z positions in **Fig.4e**. The damage density shows a clearly depth-dependent pattern, which indicates that the degree of the cathode damage is not uniform. The degree of cracking gradually decreases and tends to become stable as the distance from the separator increases.

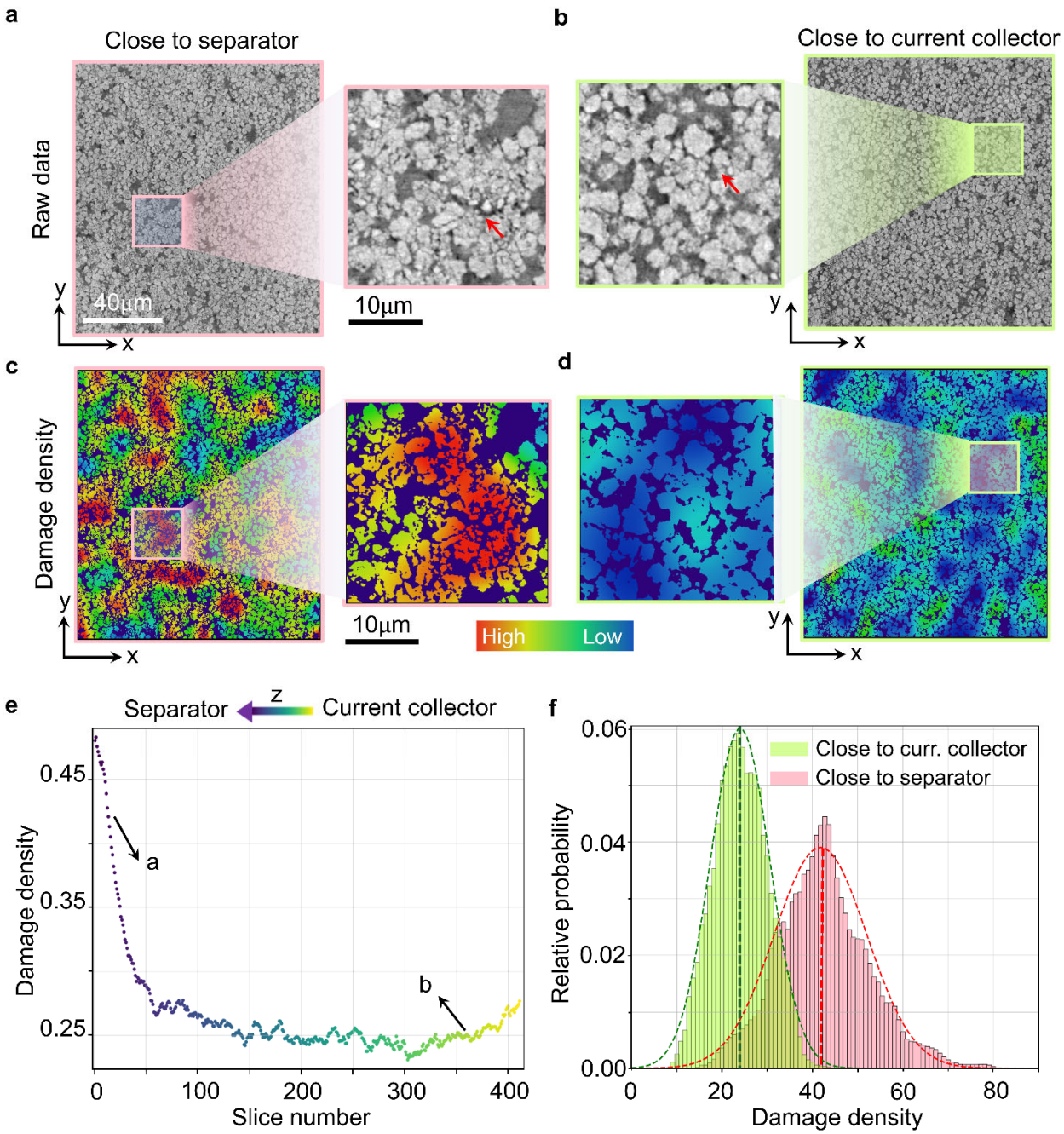

Fig. 4. Quantification of heterogeneous degradation in composite battery cathode. (a) and (b) Two slices that are close to the separator and the current collector, respectively. Small regions are magnified for better visuallization. Arrows point to the cathode fractures. (c) and (d) are the corresponding damage density map of (a) and (b) respectively. (e) The

cracking profile as a function of the depth, i.e., the z positions. (f) Comparison of the probability distribution of the particle damages in (a) and (b).

In addition to the depth-dependent cracking profile, which is a 1D representation of the inhomogeneous degree of active material utilization at the electrode level, our imaging data also offer valuable insights into the lateral and, more importantly, the spatial complexity. This is shown in the damage density maps in **Fig.4c** and **4d**. It is observed that the slice near the seperator is populated with red and yellow regions, while more green and blue regions can be seen near the current collector. We further plot the probability distributions of the damage degrees over these two slices in **Fig.4f.** A clear peak shift between these two distributions can be clearly seen.

A similar finding of the depth-dependent cathode fracturing has been reported in our previous studies [7,21] for the electrode made of spherical secondary NMC particles in a coin cell configuration. This consistency suggests that the electrochemical polarization effect is ubiquitous, regardless of the particle morphology and cell configuration.

3.4 Association of particle cracks with energy density

The mechanical damage on particles and electrodes is clearly detrimental. Engineering efforts are needed to improve the robustness of individual particles and to formulate a better strategy for packing the particles together. Generally speaking, the particle packing density is positively correlated with the effective energy density. However, a balance between the energy density and the life time shall be carefully considered as we will demonstrate, in this work, that their interplay is rather sophisticated.

To gain further insights, we conduct a statistical analysis on the relationship between the packing density and the damage degree in the imaged cathode. In addition to the crack density maps, we calculate the corresponding particle densities. In **Figs.5a-d**, the maps of damage density and particle density are shown for two slices at different depth. **Fig. 5e** shows the correlation plot between particle density and damage density for the entire imaged electrode. Overall, as the particle density increases, the particles exhibit a severer mechanical damage, which is supported by the fitted line with positive slope. This may be because regions with dense particle packing could experience a larger local current density, which leads to an over-used effect as well as a higher probability of side reactions during battery cycling.

However, if we look at the spatial density maps in **Figs.5a-d**, there exists interesting patterns between these two different slices. For the slice close to the current collector, the particle density map positively correlates with the damage density map, which aligns with the overall trend. For the slice close to separator, however, regions having less particles show higher damage. This phenomenon is further illustration by **Fig. 5f**, where the correlations between particle density and damage density are plotted layer-by-layer from the slice close to current collector to those close to separator. This is an very interesting observation and we provide a plausible narrative here. Near the electrode surface close to the separator, the overpotentials are larger. Therefore if the particle packing is low, only few particles undergo the reaction of Li (de)intercalation with high kinetic rate. This should stress the crystalline structure and trigger the particle cracking. If many particles are present, instead, the reaction occurs more diffusively so that the local overpotential is lower and the kinetics less impactful.

These results indicate that, in order to reduce the particle cracks, adaptive strategies of particle packing density for different depth should be considered. That is to say, for the top layer close to the separator, larger particle packing density may be used to reduce the overall particle cracks. Overall, a structural gradient throughout the depth of the electrode may be necessary for a global optimization.

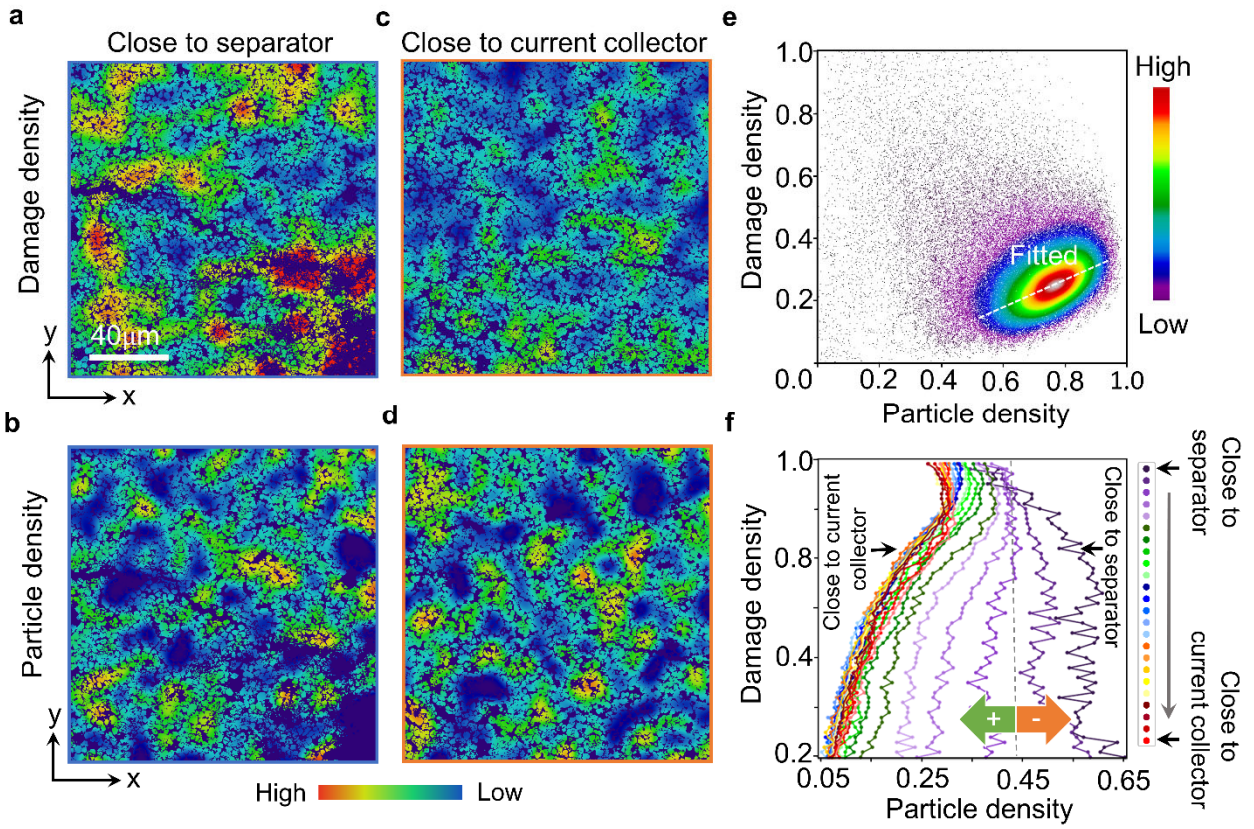

Fig. 5. Association of particle cracks with energy density. (a) and (b) Damage density map and particle density map of a slice close to the separator. (c) and (d) Damage density map and particle density map of a slice close to the current collector. (e) The correlation plot of particle density and damage density over the entire imaged 3D volume. The overall positive trend is indicated by the white fitted line. (f) The correlation between particle

density and damage density is plotted layer-by-layer. A positive-to-negative transition is observed.

Conclusion

Particle and electrode cracking in Li-ion battery cathode has been broadly observed, yet its mechanisms and behavior have not been completely understood. Several strategies have been proposed to resolve this problem, such as reducing the particle size and introducing electrolyte additives. However, the investigation of cathode particle and electrode cracks in realistic cells is time-consuming and subjective to manual interpretation of the complicated imaging data. Thus, we develop a deep learning-based approach to automatically extract the crack patterns of a commercial 18650-type battery cathode. Our method quantifies the 3D reconstructions obtained by nanoscale hard X-ray phase-contrast holotomography. The damage heterogeneity in the imaged cathode is quantified with statistical significance. The association between the damage density and particle packing density provides a potential viable approach to globally optimized the structural robustness by adaptively incorporate a depth-dependent structural gradient. This work also highlights the effectiveness of advanced machine learning approaches to accelerate the imaging data analysis for energy materials science.

Reference

[1] L. Mu, R. Lin, R. Xu, L. Han, S. Xia, D. Sokaras, J.D. Steiner, T.-C. Weng, D. Nordlund, M.M. Doeff, Y. Liu, K. Zhao, H.L. Xin, F. Lin, Oxygen Release Induced Chemomechanical Breakdown of Layered Cathode Materials, Nano Lett. 18 (2018) 3241–3249. https://doi.org/10.1021/acs.nanolett.8b01036.

[2] P. Yan, J. Zheng, M. Gu, J. Xiao, J.-G. Zhang, C.-M. Wang, Intragranular cracking as a critical barrier for high-voltage usage of layer-structured cathode for lithium-ion batteries, Nat Commun. 8 (2017) 14101. https://doi.org/10.1038/ncomms14101.

[3] H.-H. Ryu, K.-J. Park, C.S. Yoon, Y.-K. Sun, Capacity Fading of Ni-Rich Li[Ni x Co y Mn1–x–y]O2 (0.6 ≤ x ≤ 0.95) Cathodes for High-Energy-Density Lithium-Ion Batteries: Bulk or Surface Degradation?, Chem Mater. 30 (2018) 1155–1163. https://doi.org/10.1021/acs.chemmater.7b05269.

[4] H. Kim, M.G. Kim, H.Y. Jeong, H. Nam, J. Cho, A New Coating Method for Alleviating Surface Degradation of LiNi0.6Co0.2Mn0.2O2 Cathode Material: Nanoscale Surface Treatment of Primary Particles, Nano Lett. 15 (2015) 2111–2119. https://doi.org/10.1021/acs.nanolett.5b00045.

[5] G. Qian, F. Monaco, D. Meng, S.-J. Lee, G. Zan, J. Li, D. Karpov, S. Gul, D. Vine, B. Stripe, J. Zhang, J.-S. Lee, Z.-F. Ma, W. Yun, P. Pianetta, X. Yu, L. Li, P. Cloeten, Y. Liu, The role of structural defects in commercial lithium-ion batteries, Cell Reports Phys Sci. (2021) 100554. https://doi.org/10.1016/j.xcrp.2021.100554.

[6] G. Zan, J. Zhang, F. Monaco, S. Gul, G. Qian, J. Li, D.J. Vine, P. Cloetens, W. Yun, P. Pianetta, Y. Liu, Understanding multi-scale battery degradation with a macro-to-nano zoom through its hierarchy, J Mater Chem A. 9 (2021) 19886–19893. https://doi.org/10.1039/d1ta02262h.

[7] Z. Jiang, J. Li, Y. Yang, L. Mu, C. Wei, X. Yu, P. Pianetta, K. Zhao, P. Cloetens, F. Lin, Y. Liu, Machine-learning-revealed statistics of the particle-carbon/binder detachment in lithium-ion battery cathodes, Nature Communications. 11 (2020) 2310. https://doi.org/10.1038/s41467-020-16233-5.

[8] O. Ronneberger, P. Fischer, T. Brox, U-Net: Convolutional Networks for Biomedical Image Segmentation, in: Medical Image Computing and Computer-Assisted Intervention, 2015: pp. 234–241.

[9] Y. Yang, R. Xu, K. Zhang, S. Lee, L. Mu, P. Liu, C.K. Waters, S. Spence, Z. Xu, C. Wei, D.J. Kautz, Q. Yuan, Y. Dong, Y. Yu, X. Xiao, H. Lee, P. Pianetta, P. Cloetens, J. Lee, K. Zhao, F. Lin, Y. Liu, Quantification of Heterogeneous Degradation in Li-Ion Batteries, Adv Energy Mater. 9 (2019) 1900674. https://doi.org/10.1002/aenm.201900674.

[10] R. Xu, Y. Yang, F. Yin, P. Liu, P. Cloetens, Y. Liu, F. Lin, K. Zhao, Heterogeneous damage in Li-ion batteries: Experimental analysis and theoretical modeling, J Mech Phys Solids. 129 (2019) 160–183. https://doi.org/10.1016/j.jmps.2019.05.003.

[11] Y. Liu, J. Nelson, C. Holzner, J.C. Andrews, P. Pianetta, Recent advances in synchrotron-based hard x-ray phase contrast imaging, J Phys D Appl Phys. 46 (2013) 494001. https://doi.org/10.1088/0022-3727/46/49/494001.

[12] P. Cloetens, W. Ludwig, J. Baruchel, D.V. Dyck, J.V. Landuyt, J.P. Guigay, M. Schlenker, Holotomography: Quantitative phase tomography with micrometer resolution using hard synchrotron radiation x rays, Appl Phys Lett. 75 (1999) 2912–2914. https://doi.org/10.1063/1.125225.

[13] A. Mirone, E. Brun, E. Gouillart, P. Tafforeau, J. Kieffer, The PyHST2 hybrid distributed code for high speed tomographic reconstruction with iterative reconstruction and a priori knowledge capabilities, Nucl Instruments Methods Phys Res Sect B Beam Interactions Mater Atoms. 324 (2014) 41–48. https://doi.org/10.1016/j.nimb.2013.09.030.

[14] G. Balakrishnan, A. Zhao, M.R. Sabuncu, J. Guttag, A.V. Dalca, VoxelMorph: A Learning Framework for Deformable Medical Image Registration, Ieee T Med Imaging. 38 (2019) 1788–1800. https://doi.org/10.1109/tmi.2019.2897538.

[15] V. Badrinarayanan, A. Kendall, R. Cipolla, SegNet: A Deep Convolutional Encoder-Decoder Architecture for Image Segmentation, Ieee T Pattern Anal. 39 (2015) 2481–2495. https://doi.org/10.1109/tpami.2016.2644615.

[16] H.R. Lee, L. Liao, W. Xiao, A. Vailionis, A.J. Ricco, R. White, Y. Nishi, W. Chiu, S. Chu, Y. Cui, Three-Dimensional Analysis of Particle Distribution on Filter Layers inside N95 Respirators by Deep Learning, Nano Lett. 21 (2021) 651–657. https://doi.org/10.1021/acs.nanolett.0c04230.

[17] E. Moen, D. Bannon, T. Kudo, W. Graf, M. Covert, D.V. Valen, Deep learning for cellular image analysis, Nat Methods. 16 (2019) 1233–1246. https://doi.org/10.1038/s41592-019-0403-1.

[18] B. Xu, N. Wang, T. Chen, M. Li, Empirical Evaluation of Rectified Activations in Convolutional Network, Arxiv. (2015).

[19] A. Krizhevsky, I. Sutskever, G.E. Hinton, ImageNet classification with deep convolutional neural networks, Commun Acm. 60 (2017) 84–90. https://doi.org/10.1145/3065386.

[20] P. Isola, J.-Y. Zhu, T. Zhou, A.A. Efros, Image-to-Image Translation with Conditional Adversarial Networks, 2017 Ieee Conf Comput Vis Pattern Recognit Cvpr. (2017) 5967–5976. https://doi.org/10.1109/cvpr.2017.632.

[21] S. Xia, L. Mu, Z. Xu, J. Wang, C. Wei, L. Liu, P. Pianetta, K. Zhao, X. Yu, F. Lin, Y. Liu, Chemomechanical interplay of layered cathode materials undergoing fast charging in lithium batteries, Nano Energy. 53 (2018) 753–762. https://doi.org/10.1016/j.nanoen.2018.09.051.

Data availability

The data supporting the findings of the study is available at the GitHub repository: https://github.com/SSRL-LiuGroup.

Author contributions

T. Fu and F. Monaco contributed equally to this work. Y. Liu conceived the study. K. Zhang, Q. Yuan, P. Pianetta and P. Cloetens contributed to the interpretation of the data.

T. Fu, F. Monaco, J. Li and Y. Liu wrote the manuscript with valuable input from all coauthors.

Conflicts of interest

The authors declare no conflicts of interest.